European Congress on Computational Methods in Applied Sciences and Engineering
ECCOMAS 2000
Barcelona, 11-14 September 2000

NUMERICAL SIMULATION OF COUPLED LIQUID-SOLID DYNAMICS

Jeroen Gerrits and Arthur E.P. Veldman

University of Groningen, Department of Mathematics
P.O. Box 800, 9700 AV Groningen, The Netherlands
e-mail: j.gerrits@math.rug.nl, a.e.p.veldman@math.rug.nl

Key words: Coupled dynamics, Flat spin, Free-surface flow, Micro-gravity.

Abstract. *Under micro-gravity conditions, fluid behaviour is — at least from a computational point of view — more complicated than under terrestrial conditions. Since capillary forces at the free surface dominate the flow, the location and shape of the free surface have to be computed accurately. Moreover, in an extra-terrestrial environment, fluid has the tendency to undergo large topological changes requiring an accurate and robust method for free-surface advection.*

Further, the fluid is often contained in a cavity (e.g. satellite) that itself is moving; not only because of external forces (e.g. manoeuvring thrusters on a satellite), but also under influence of the fluid motion: the dynamics of the solid body motion and the liquid motion are coupled.

In this paper we present a method for simulating coupled liquid-solid dynamics. For the liquid dynamics (the first part of this paper) we solve the Navier-Stokes equations on a Cartesian grid; complex geometries are handled using a cut-cell approach. Transportation of the free surface is based on the VOF-method, but is adapted with a local height function in order to avoid 'flotsam' and 'jetsam'. In the second part of this paper we discuss the coupling between the liquid- and solid body motion. Care has to be taken in integrating the coupled equations in order to keep the numerical method stable for arbitrary liquid/solid mass ratios.

Finally, the free-flying satellite SloshSat will be introduced. SloshSat is scheduled for launch in the year 2001 and is designed to investigate liquid dynamics and the coupled liquid-solid dynamics under micro-gravity conditions. The results of this mission promise to provide valuable validation material for Computational Fluid Dynamics methods.

1 INTRODUCTION

With the ongoing increase of computer resources as well as the improvement of numerical algorithms, experimental studies of fluid flow are more and more accompanied (or even replaced) by numerical simulations. Especially within the area of extra-terrestrial fluid flow, Computational Fluid Dynamics (CFD) has become essential, since, on earth, a micro-gravity environment can be attained for a few seconds only (e.g. during a parabolic flight or in a drop tower). Nevertheless, experiments remain crucial for validation of CFD codes and better physical understanding of liquid motion in space. Hence, the launch of the experiment satellite SloshSat (early in 2001) is a great opportunity for comparing simulation results and experiment results. SloshSat is a small free-flying satellite containing an experiment tank which is partially filled with water. It will perform a number of manoeuvres in order to study the liquid motion in an environment where capillary forces are dominant. Moreover, the dynamical interaction between the liquid motion and the motion of the satellite itself will be investigated.

In 1995 we started the development of a CFD code, called ComFlo, which is currently able to simulate the SloshSat experiment scenario. Thus, it can simulate extra-terrestrial free-surface flow in three-dimensional complex geometries taking into account the interaction between the liquid motion and the solid body motion. As a spin-off, the code is capable of handling terrestrial flows (i.e. gravity dominated) [1] and flows without the presence of a free surface.

In our method we solve the (incompressible) Navier-Stokes equations, using a finite-volume method, on a stationary Cartesian mesh, thus avoiding the time-consuming grid generation of a body-fitted mesh. To be able to handle arbitrary complex geometries we make use of a cut-cell approach. In this method the flow domain is simply cut out of the Cartesian mesh, hereby creating irregular cells near the boundary of the flow domain. If these cells become small, severe time-step restrictions may occur [2]. By applying the boundary conditions in a more symmetric manner, in our method, we overcome these restrictions. The free surface is described by a Volume-of-Fluid function which can be regarded as the discrete indicator function of the fluid. Transportation of the free surface is based on the well-known Volume-of-Fluid (VOF) method by Hirt and Nichols [3]. However, in the standard VOF method small bits of fluid may get (unphysically) separated from the main body of fluid ("flotsam" and "jetsam") [4]. In our method we avoid this by advecting the free surface using a local height function. The mathematical and numerical modeling of the liquid dynamics will be discussed in section 2.

As mentioned before, we also take the interaction between the motion of the fluid and the motion of the solid body (in which the fluid is contained) into account. Hereto we solve (each time step) a set of equations for the linear and angular momentum of the solid body. In these equations, of course, terms appear representing the forces and torques exerted upon the solid body by the liquid motion. On the other hand, in the Navier-Stokes equations, apparent forces exerted upon the fluid by linear and angular acceleration and

rotation of the solid body must be added which makes the interaction complete. Some care has to be taken in integrating the coupled equations, since a naive integration would result in an unstable method when the liquid mass becomes too large with respect to the solid body mass [5]. In our method the system is stable for any liquid/solid mass ratio. The modeling of the coupled dynamics is explained in detail in section 3.

2 LIQUID DYNAMICS

In this section we discuss the mathematical and numerical modeling of the liquid dynamics. First the governing equations are stated. Then the main features of the numerical method are highlighted.

2.1 Governing equations

The motion of an incompressible fluid with density ρ and molecular viscosity μ is governed by conservation of mass

$$\nabla \cdot \boldsymbol{u} = 0, \tag{1}$$

and conservation of momentum (the Navier-Stokes equations)

$$\frac{\partial \boldsymbol{u}}{\partial t} + \nabla \cdot \left(\boldsymbol{u}\boldsymbol{u}^T \right) = -\frac{1}{\rho} \left(\nabla p - \mu \left(\nabla \cdot \nabla \right) \boldsymbol{u} \right), \tag{2}$$

in which $\boldsymbol{u} = (u, v, w)^T$ is the velocity vector and p the pressure.

At the free surface we need boundary conditions for the velocity and the pressure. First, as a boundary condition for the velocity, we assume that the void exerts no tangential force on the fluid, i.e.

$$\mu \left(\frac{\partial u_n}{\partial \boldsymbol{t}} + \frac{\partial u_t}{\partial \boldsymbol{n}} \right) = 0, \tag{3}$$

where $u_n = \boldsymbol{u} \cdot \boldsymbol{n}$ and $u_t = \boldsymbol{u} \cdot \boldsymbol{t}$ are the velocities normal and tangential to the free surface respectively. The boundary condition for the pressure follows from a balance of normal forces (from pressure, surface tension and viscous effects) at the free surface

$$p - \mu \frac{\partial u_n}{\partial \boldsymbol{n}} = p_0 - \sigma \kappa. \tag{4}$$

In this equation p_0 is the void pressure and σ and κ are the surface tension and total curvature of the free surface respectively. Usually, the second term on the left-hand side of equation (4) is ignored, since it is small compared to the other terms. Finally, at the solid boundary, we assume that the velocity vanishes, i.e. $\boldsymbol{u} = 0$ (no-slip condition).

2.2 Apertures and labeling

As mentioned before, we discretize the governing equations on a Cartesian grid. To be able to handle complex geometries on such a grid, we introduce so-called apertures.

These are numbers between zero and one, indicating the fractional volume (or area) of a cell (or cell face) that is open for flow. We denote the volume aperture of a cell by F^b and the edge apertures of a cell face perpendicular to the x-, y- and z-axis by A^x, A^y and A^z respectively. Yet another volume aperture F^s denotes the actual (fractional) amount of fluid present in a cell (this number is also known as the Volume-of-Fluid function). For the volume apertures we have $0 \leq F^s \leq F^b \leq 1$. Now, based on the volume apertures, we introduce cell labels. For $F^b \geq \frac{1}{2}$ three different cell types are distinguished:

E(mpty) cells. If $F^s = 0$, no fluid is present in the cell. Obviously the Navier-Stokes equations will not be discretized here.

S(urface) cells. If $F^s > 0$ and the cell has at least one empty neighbour, it will be referred to as a surface cell. In these cells equation (4) is discretized, which serves as a boundary condition for the pressure Poisson equation.

F(ull) cells. All the remaining cells are called full cells. The continuity equation (1) is discretized in every F-cell and it is combined with the discretized momentum equations (2) to form a pressure Poisson equation.

For the remaining cells, i.e. with $F^b < \frac{1}{2}$, we have a further distinction:

B(oundary) cells. In every cell having at least one neighbouring cell with $F^b \geq \frac{1}{2}$ the continuity equation is discretized as well, however, no pressure Poisson equation is formed.

(e)X(terior) cells. All remaining cells are called exterior cells and play no role in the numerical model.

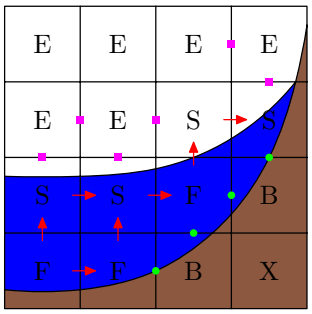

Figure 1: Labeling.

Figure 1 shows a graphical explanation of the above-mentioned. By a combination of two letters it is easy to identify labels for cell faces as well. For example, a cell face between an F- and a B-cell is labeled as FB, and so on.

Since we make use of a staggered grid (which is common in incompressible CFD), momentum equations are discretized at cell faces. Because of the pressure gradient in these equations, the momentum equations can only be discretized between two cells in which a pressure is known, i.e. at cell faces with label FF, FS and SS (the red arrows in Figure 1). As a direct consequence, in B-cells, no boundary condition for the pressure is required, since at a cell face adjacent to a B-cell no pressure gradient is computed.

With respect to stability we remark that, despite the possible occurence of very small cells, no severe time-step restrictions have to be expected. Indeed, the momentum equations are only discretized between cells with $F^b \geq \frac{1}{2}$. Thus, the discrete Navier-Stokes equations stay away from small cells. Also, this implies that some of the velocities at cell faces with label FB or SB (the green dots in Figure 1), where the no-slip boundary condition is applied, lie inside the fluid. So, on average the FB-velocities, in our method, are twice as close to — and are distributed more or less symmetrically around — the solid boundary compared to a method where all the internal velocities are solved from the Navier-Stokes equations.

More details about the discretization of the continuity equation and the Navier-Stokes equations can be found in [1, 6].

2.3 Free surface

At the free surface two boundary conditions are required, namely equation (3) for the velocity and equation (4) for the pressure. The former is applied to EE-velocities (the purple squares in Figure 1) using standard finite difference techniques. The latter is less trivial since it involves computing the curvature at the free surface, i.e. in every S-cell. Hereto a local height function is defined, e.g. $S(x, y, z) = h(x, y) - z = 0$ if the free surface is approximately horizontal (in this case h is the local height function and S is called a level-set function). Now, the total curvature is given by $\kappa = \nabla \cdot \boldsymbol{n}$, where $\boldsymbol{n} = \frac{\nabla S}{|\nabla S|}$ is the unit normal at the free surface. From a discrete point of view, the local height function is formed by adding the F^s-values in a certain column/row of cells. For example, in Figure 2, the free surface is nearly horizontal, thus a vertical height function is constructed in order to compute the curvature in the middle cell (which is a surface cell). The formula for the

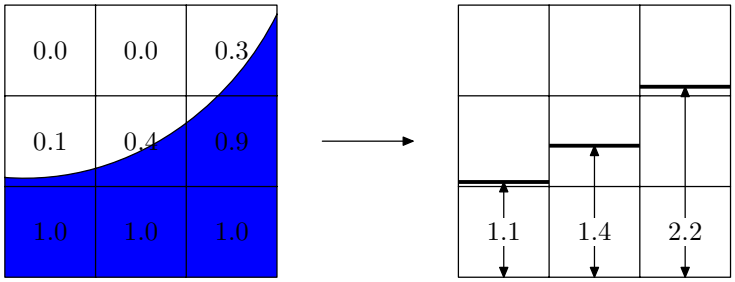

Figure 2: Local height function.

curvature is discretized using standard finite differences.

Transportation of the fluid is trivial "far" away from the free surface; the VOF-function F^s remains either zero or one. Close to the free surface the value of F^s may change from one time step to the next one. If the free surface is described by a level-set function $S(x, y, z, t) = 0$, then this function must satisfy $\frac{DS}{Dt} = 0$. For the level-set function we choose, as before, a local height function. For example, in the two-dimensional case illustrated in Figure 2, if we take $S(x, y, t) = h(x, t) - y$, then the local height in the center column at the new time step is computed by discretizing

$$\frac{DS}{Dt} = 0 \Rightarrow \frac{\partial S}{\partial t} + \boldsymbol{u} \cdot \nabla S = 0 \Rightarrow \frac{\partial h}{\partial t} = v - u\frac{\partial h}{\partial x}. \tag{5}$$

This method is an adjustment of the standard VOF-method by Hirt and Nichols and prevents that small bits of fluid get separated from the main body of fluid ("flotsam" and "jetsam").

For some results of our method with respect to the liquid dynamics we refer to [1, 6] and our web site:

`http://www.math.rug.nl/~veldman/cfd-gallery.html`

In the remaining part of this paper the emphasis will be on the coupling between the liquid- and the solid body dynamics.

3 COUPLED LIQUID-SOLID DYNAMICS

In this section we will study the interaction between the liquid motion and the motion of the solid body in which the liquid is contained. First the governing equations will be stated. Then the numerics will be discussed. In the discretization special care has to be taken in order to keep the coupling stable. This procedure will be illustrated with a simple mass-spring model. Finally, some results will be presented.

3.1 Mathematical model

The motion of the liquid is governed by equations (1) and (2). However, in the case of coupled dynamics, the motion of the solid body has to be taken into account. Hereto, we consider the liquid velocity in two reference fames: the velocity $\boldsymbol{v}$ of a liquid particle in an inertial reference frame and the velocity $\boldsymbol{u}$ of a liquid particle in a moving reference frame $Oxyz$. The relation between $\boldsymbol{u}$ and $\boldsymbol{v}$ is given by [7]

$$\frac{D\boldsymbol{v}}{Dt} = \dot{\boldsymbol{q}} + \frac{d\boldsymbol{\omega}}{dt} \times \boldsymbol{r} + \boldsymbol{\omega} \times (\boldsymbol{\omega} \times \boldsymbol{r}) + \frac{D\boldsymbol{u}}{Dt} + 2\boldsymbol{\omega} \times \boldsymbol{u}, \tag{6}$$

where $\dot{\boldsymbol{q}} = d\boldsymbol{q}/dt + \boldsymbol{\omega} \times \boldsymbol{q}$ is the acceleration of the moving origin O with respect to the inertial reference frame, $\boldsymbol{\omega}$ is the angular rate of the moving reference frame $Oxyz$ and $\boldsymbol{r}$

is the position of the liquid particle in $Oxyz$. Now, the Navier-Stokes equations take the form

$$\frac{D\boldsymbol{v}}{Dt} = -\frac{1}{\rho}\left(\nabla p - \mu\left(\nabla\cdot\nabla\right)\boldsymbol{u}\right). \tag{7}$$

This equation, combined with the continuity equation (1), describes the motion of the liquid.

The model for the solid body motion consists of an equation for linear momentum

$$m_s\dot{\boldsymbol{q}} + \frac{d\boldsymbol{\omega}}{dt}\times m_s\overline{\boldsymbol{r}}_s + \boldsymbol{\omega}\times\left(\boldsymbol{\omega}\times m_s\overline{\boldsymbol{r}}_s\right) = \mathcal{F}, \tag{8}$$

and an equation for angular momentum

$$m_s\overline{\boldsymbol{r}}_s\times\dot{\boldsymbol{q}} + \boldsymbol{I}_s\frac{d\boldsymbol{\omega}}{dt} + \boldsymbol{\omega}\times\boldsymbol{I}_s\boldsymbol{\omega} = \mathcal{T}, \tag{9}$$

where $\mathcal{F}$ and $\mathcal{T}$ are respectively the force and torque (due to pressure and viscous effects) that the fluid exerts on the boundary of the solid body, i.e.

$$\mathcal{F} = \oint_{\partial V}\left(p\boldsymbol{I}_3 - \mu\nabla\boldsymbol{u}\right)\cdot\boldsymbol{n}\,dS = -\int_V \rho\frac{D\boldsymbol{v}}{Dt}\,dV, \tag{10}$$

$$\mathcal{T} = \oint_{\partial V}\left(\boldsymbol{r}\times\left(p\boldsymbol{I}_3 - \mu\nabla\boldsymbol{u}\right)\right)\cdot\boldsymbol{n}\,dS = -\int_V \rho\boldsymbol{r}\times\frac{D\boldsymbol{v}}{Dt}\,dV. \tag{11}$$

Here we used the divergence theorem and equation (7). Further $\boldsymbol{I}_3$ is the 3×3 identity matrix and $\boldsymbol{n}$ the outward pointing normal at the boundary ∂V of the total volume V of the solid body. In equations (8) and (9) the unknown variables are $d\boldsymbol{q}/dt$ and $d\boldsymbol{\omega}/dt$, representing the linear and angular acceleration of the solid body motion respectively. The mass of the solid body is denoted by m_s. Further, $\boldsymbol{I}_s$ is the moment of inertia tensor and $\overline{\boldsymbol{r}}_s$ is the center of mass of the solid body. Note that the latter two quantities are relative to the moving reference frame.

Before discretizing the equations for the solid body motion we are going to study the stability of the numerical coupling using a simple mass-spring model.

3.2 Mass-spring model

Consider, as shown in Figure 3, a system of two masses m_s and m_l, representing the solid body mass and the liquid mass respectively. These masses are connected with each other by a spring having a spring constant k and length ℓ. If the system is partitioned such as indicated by the dashed rectangles in Figure 3, then the equations of motion read

$$\begin{aligned} m_s\,\ddot{x}_s &= -F, \\ m_l\,\ddot{x}_l &= F, \\ k\left(x_l - x_l - \ell\right) &= -F. \end{aligned}$$

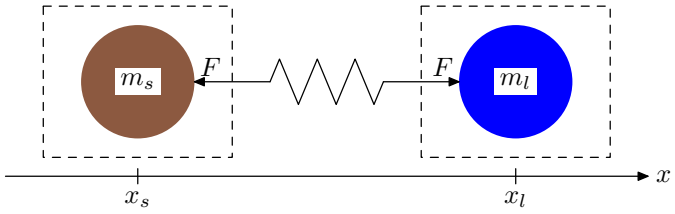

Figure 3: Partition of mass-spring system (possibly unstable coupling).

Now, in solving these equations iteratively (a superscript will denote the level of iteration), assume that the solid body moves in reaction to the liquid responsive forces. Then the system becomes

$$m_s \ddot{x}_s^{(n+1)} = -F^{(n)}, \tag{12}$$

$$F^{(n+1)} - m_l \ddot{x}_l^{(n+1)} = 0, \tag{13}$$

$$\frac{1}{k} F^{(n+1)} + x_l^{(n+1)} = \ell + x_s^{(n+1)}. \tag{14}$$

It is easy to see that the variables x_s and x_l can be eliminated from these equations, which results in

$$\frac{m_l}{k} \ddot{F}^{(n+1)} + F^{(n+1)} = -\frac{m_l}{m_s} F^{(n)}. \tag{15}$$

If the coupling is infinitely stiff, i.e. $k = \infty$, then the iterations converge if and only if $m_l/m_s < 1$. Thus the coupling is numerically unstable if the liquid mass exceeds the solid mass. Note that, for an infinitely stiff coupling, this result does not depend on the discretization method of the time derivative or the size of the time step.

In order to overcome these stability problems we follow a method that was developed for aerodynamical flow [8]. The idea is to treat a frozen state of the liquid simultaneously with the solid mass, which is graphically illustrated in Figure 4. Mathematically spoken, this means adding a term $m_l \ddot{x}_s^{(n+1)}$ to the left-hand side of equation (12). This term is also added to the right-hand side, however, this time with iteration level n, now representing (small) oscillations of the fluid around the frozen state. Thus, instead of equation (12)

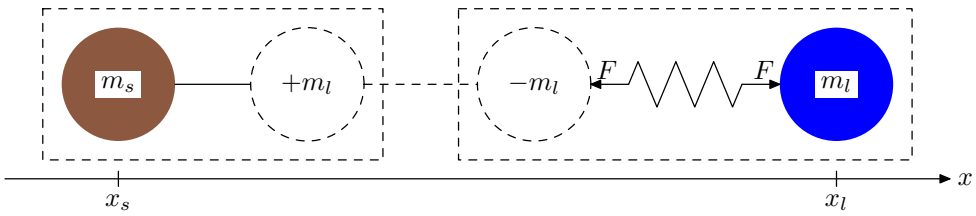

Figure 4: Partition of mass-spring system (stable coupling).

we use

$$(m_s + m_l)\,\ddot{x}_s^{(n+1)} = -F^{(n)} + m_l\,\ddot{x}_s^{(n)}. \tag{16}$$

Combining this equation with equations (13) and (14) and eliminating, again, x_s and x_l results in

$$\frac{m_l}{k}\ddot{F}^{(n+1)} + F^{(n+1)} = \frac{m_l}{m_s + m_l}\frac{m_l}{k}\ddot{F}^{(n)}. \tag{17}$$

Compared to equation (15) the right-hand side has changed; the important difference is the presence of a factor $m_l/(m_s + m_l)$ (which is always less than one) in equation (17) instead of a factor m_l/m_s in equation (15).

The stability analysis of the mass-spring model that has been discussed in this section can be made more precise, but in this paper we only wanted to sketch the idea that will be used in the next section.

3.3 Numerical model

In this section we will discuss the discretization of the equations for the solid body motion. Before doing this, we note that on the left-hand side of equations (8) and (9) only the mass m_s of the solid body appears, similar to the partition of the mass-spring model in the previous section that resulted in a — numerically speaking — possibly unstable coupling. In the previous section we also saw the solution for this problem: on the left-hand side of the equation for the solid body motion the total mass $m = m_s + m_l$ of the coupled system should appear. This can be achieved for equation (8), for example, by using equation (6):

$$\begin{aligned}
\int_V \rho\frac{D\boldsymbol{v}}{Dt}\,dV &= \int_V \rho\left(\dot{\boldsymbol{q}} + \frac{d\boldsymbol{\omega}}{dt}\times\boldsymbol{r} + \boldsymbol{\omega}\times(\boldsymbol{\omega}\times\boldsymbol{r})\right)dV + \underbrace{\int_V \rho\left(\frac{D\boldsymbol{u}}{Dt} + 2\boldsymbol{\omega}\times\boldsymbol{u}\right)dV}_{\mathcal{I}} \\
&= \dot{\boldsymbol{q}}\int_V \rho\,dV + \frac{d\boldsymbol{\omega}}{dt}\times\int_V \rho\boldsymbol{r}\,dV + \boldsymbol{\omega}\times\left(\boldsymbol{\omega}\times\int_V \rho\boldsymbol{r}\,dV\right) + \mathcal{I} \\
&= m_l\dot{\boldsymbol{q}} + \frac{d\boldsymbol{\omega}}{dt}\times m_l\overline{\boldsymbol{r}}_l + \boldsymbol{\omega}\times(\boldsymbol{\omega}\times m_l\overline{\boldsymbol{r}}_l) + \mathcal{I}.
\end{aligned}$$

In this equation m_l and $\overline{\boldsymbol{r}}_l$ denote the liquid mass and the center of mass of the liquid respectively. Combining this equation with equations (8) and (10) results in

$$m\dot{\boldsymbol{q}} + \frac{d\boldsymbol{\omega}}{dt}\times m\overline{\boldsymbol{r}} + \boldsymbol{\omega}\times(\boldsymbol{\omega}\times m\overline{\boldsymbol{r}}) = -\int_V \rho\left(\frac{D\boldsymbol{u}}{Dt} + 2\boldsymbol{\omega}\times\boldsymbol{u}\right)dV \tag{18}$$

A similar analysis can be done for equations (9) and (11) which results in

$$m\overline{\boldsymbol{r}}\times\dot{\boldsymbol{q}} + \boldsymbol{I}\frac{d\boldsymbol{\omega}}{dt} + \boldsymbol{\omega}\times\boldsymbol{I}\boldsymbol{\omega} = -\int_V \rho\boldsymbol{r}\times\left(\frac{D\boldsymbol{u}}{Dt} + 2\boldsymbol{\omega}\times\boldsymbol{u}\right)dV. \tag{19}$$

In these equations $m = m_s + m_l$ is the total mass, $\boldsymbol{I} = \boldsymbol{I}_s + \boldsymbol{I}_l$ the moment of inertia tensor of the coupled system and $\overline{\boldsymbol{r}} = (m_s\overline{\boldsymbol{r}}_s + m_l\overline{\boldsymbol{r}}_l)/m$ the center of mass of the coupled system. Note that the latter two quantities are time dependent because of the sloshing liquid. Equations (18) and (19) are of the desired form, in which the total mass m appears on the left-hand side, that results in a stable numerical coupling for arbitrary liquid/solid mass ratios.

The time discretization of the equations for linear momentum (18) and angular momentum (19) is straightforward: the unknown variables $d\boldsymbol{q}/dt$ and $d\boldsymbol{\omega}/dt$ are discretized at the new time level; the rest is evaluated at the old time level. In short, this can be written as

$$m\frac{d\boldsymbol{q}}{dt}^{n+1} + \frac{d\boldsymbol{\omega}}{dt}^{n+1} \times m\overline{\boldsymbol{r}}^n = \mathcal{L}^n, \tag{20}$$

$$m\overline{\boldsymbol{r}}^n \times \frac{d\boldsymbol{q}}{dt}^{n+1} + \boldsymbol{I}^n\frac{d\boldsymbol{\omega}}{dt}^{n+1} = \mathcal{A}^n, \tag{21}$$

where we used $\dot{\boldsymbol{q}} = d\boldsymbol{q}/dt + \boldsymbol{\omega}\times\boldsymbol{q}$. The spatial discretization of these equations will not be discussed here, since it involves standard discretization techniques only. We just remark that the terms containing integrals over the total volume V can be computed using the VOF-function F^s, e.g.

$$\int_V \varphi^n \, dV = \sum_{i,j,k} \varphi^n_{i,j,k} F^s_{i,j,k} h_i h_j h_k, \tag{22}$$

where φ is some scalar variable and the summation is over the grid cells and $h_i h_j h_k$ is the volume of the cell with index (i, j, k).

The 6×6 linear system for the unknown vectors $(d\boldsymbol{q}/dt)^{n+1}$ and $(d\boldsymbol{\omega}/dt)^{n+1}$ that is formed by equations (20) and (21) is solved by Gaussian elimination.

4 RESULTS

In this section we will show some results of our method. First, we will validate the method in the absence of liquid, i.e. pure solid body motion. Then the numerical stability will be checked by studying different liquid mass ratios m_l/m in the so-called flat spin. Also, the effect of the liquid mass ratio and the time step on the results will be investigated.

4.1 Empty tank

As a first validation test we consider the motion of an empty tank, e.g. a beam with dimensions $a \times b \times c$. If we take the center of mass of the tank as the origin of the coordinate system $Oxyz$, i.e. $\overline{\boldsymbol{r}} = 0$, then the equations (18) and (19) reduce to

$$\begin{aligned} m_s\dot{\boldsymbol{q}} &= 0, \\ \boldsymbol{I}_s\frac{d\boldsymbol{\omega}}{dt} + \boldsymbol{\omega}\times\boldsymbol{I}_s\boldsymbol{\omega} &= 0. \end{aligned} \tag{23}$$

The first equation expresses that the tank moves with constant linear velocity. The second equation describes the evolution of the angular velocity $\boldsymbol{\omega} = (\omega_x, \omega_y, \omega_z)^T$. If the axes of $Oxyz$ are aligned with the axes of the tank, then the moment of inertia tensor is a diagonal matrix $\boldsymbol{I}_s = \mathrm{diag}\,(I_{xx}, I_{yy}, I_{zz}) = \frac{1}{12} m_s \mathrm{diag}\,((b+c)^2, (a+c)^2, (a+b)^2)$ (note that in the case of an empty tank, the moment of inertia tensor does not depend on time). Thus, equation (23) simplifies to three equations

$$\frac{d\omega_x}{dt} = \frac{I_{yy} - I_{zz}}{I_{xx}}\,\omega_y\omega_z, \quad \frac{d\omega_y}{dt} = \frac{I_{zz} - I_{xx}}{I_{yy}}\,\omega_x\omega_z, \quad \frac{d\omega_z}{dt} = \frac{I_{xx} - I_{yy}}{I_{zz}}\,\omega_x\omega_y. \tag{24}$$

We can drive the system by choosing initial values $\boldsymbol{\omega}^0 = \left(\omega_x^0, \omega_y^0, \omega_z^0\right)^T$ for the angular velocity. If two components are chosen equal to zero, then the system keeps rotating with the initial angular velocity. So, to make it more interesting, we choose $\boldsymbol{\omega}^0 = (2, 0, 1)^T$. Further, the moment of inertia tensor is set to $\boldsymbol{I} = \mathrm{diag}(1, 1, 2\pi + 1)$ (note that also in the case $I_{xx} = I_{yy} = I_{zz}$ the system keeps rotating with the initial angular velocity). With these conditions the solution can be found analytically, namely

$$\omega_x(t) = 2\cos(2\pi t), \quad \omega_y(t) = 2\sin(2\pi t), \quad \omega_z(t) = 1. \tag{25}$$

The results of the simulation are shown in Figure 5. The dashed lines show the error

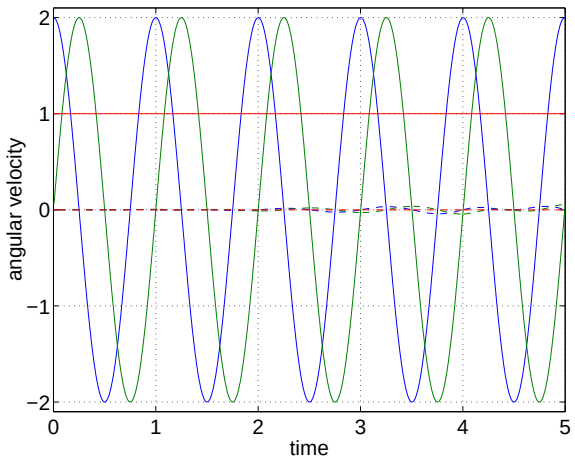

Figure 5: Angular velocities of the x- (blue), y- (green) and z-axis(red) of a rotating empty tank with $\boldsymbol{\omega}^0 = (2, 0, 1)^T$ and $\boldsymbol{I} = \mathrm{diag}(1, 1, 2\pi + 1)$. The dashed lines show the error from the analytical solution.

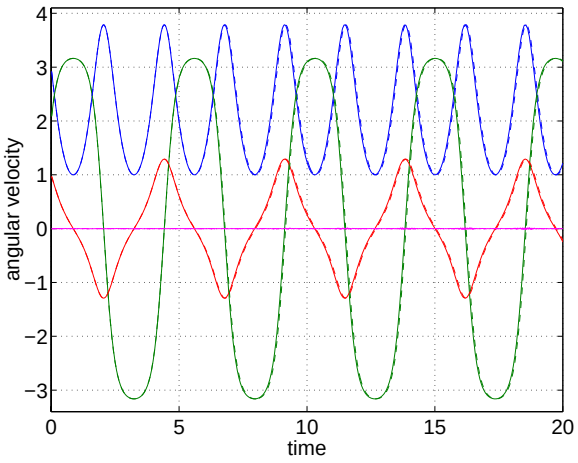

Figure 6: Same as in Figure 5 but now with $\boldsymbol{\omega}^0 = (3, 2, 1)^T$ and $\boldsymbol{I} = \mathrm{diag}(1, 2, 4)$. The solid lines and dashed lines correspond to time steps that differ a factor of two.

from the analytical solution. In Figure 6 the results of another simulation with an empty tank are shown. In this case we chose $\boldsymbol{\omega}^0 = (3, 2, 1)^T$ and $\boldsymbol{I} = \mathrm{diag}(1, 2, 4)$ which led to a

nonlinear system of equations. Actually in this figure the results of two simulations are shown of which the time steps differ a factor of two. The purple line represents the kinetic energy of the rotating tank (from which the initial kinetic energy has been subtracted) that remains constant during the simulation.

4.2 Flat spin

In this section the tank will be filled with liquid, thus demonstrating the capabilities of the full interaction model.

Consider a rectangular tank with dimensions $6 \times 4 \times 2$, now completely filled with liquid. Both the tank mass m_s and the density ρ of the liquid are set to unity. This implies that the mass of the liquid is equal to $m_l = 48$, thus the liquid mass is nearly 98% of the total mass. With these conditions the z-axis is the axis of maximum moment of inertia. Initially the tank rotates around the x-axis with an angular velocity of 10, while the angular velocities around the y- and z-axis are zero. Since both the x- and y-axis are unstable and because of the viscous damping by the liquid the system will settle itself into a steady state in which the tank rotates around the (stable) z-axis with constant angular velocity. This change of rotation axis from an unstable axis to a stable axis is called flat spin. In this example, the presence of liquid, which takes care of the damping, is a necessary condition for the occurence of a flat spin (remember that in the case of an empty tank no damping was observed: the system showed periodic behavior). In Figure 7 the evolution of the angular velocities around the x-, y- and z-axis is plotted.

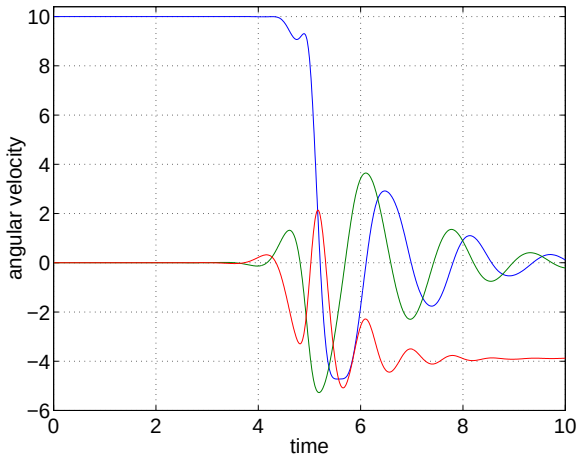

Figure 7: Angular velocities around the x- (in blue), y- (in green) and z-axis (in red) for the flat-spin simulation.

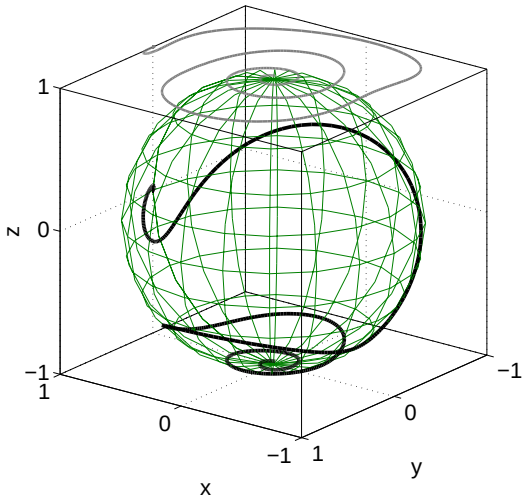

Figure 8: Graph of $\boldsymbol{\omega}/|\boldsymbol{\omega}|$ (in black) of the flat-spin simulation, showing the transition of the rotation axis. In grey the projection of this graph on the plane $z = 1$ is plotted.

Clearly, the transition from rotation around the unstable x-axis to rotation around the stable z-axis is shown. During the transition also the y-axis is excited, however, since this axis is unstable as well, the angular velocity around the y-axis vanishes eventually. The final angular velocity around the z-axis can be predicted since the total angular momentum (of the coupled system) should be conserved. In this case $\boldsymbol{I} = \boldsymbol{I}_s + \boldsymbol{I}_l = \mathrm{diag}(3, \frac{16}{3}, \frac{25}{3}) + \mathrm{diag}(80, 160, 208)$ and $\boldsymbol{\omega}^0 = (10, 0, 0)$ such that, initially, the total angular momentum is equal to $(3 + 80) \times 10 = 830$. From this it follows that the final rotation rate around the z-axis is equal to $\frac{830}{25/3+208} \approx 3.84$ in correspondence with the simulation in which the final rotation rate around this axis is equal to 3.89 (a 1.3% difference).

A more accessible way of visualizing the tank motion is shown in Figure 8. In this figure the vector $\boldsymbol{\omega}/|\boldsymbol{\omega}|$ (which is the projection of the angular velocity on the unit sphere) is plotted. From this graph the concept of flat spin — the transition from rotation around an unstable axis to rotation around the stable axis — becomes very clear.

The simulation corresponding to Figure 7 and Figure 8 was performed on a computational grid of $40 \times 30 \times 20$ cells and with a time step of 2.5×10^{-5}. Although this time step gives rise to a CFL-number in the order of 0.001 in the liquid model, this small time step turns out to be required for solving the motion of the tank accurately. Because of the small time step, this simulation took quite some time: 400000 time steps on a computational grid of $40 \times 30 \times 20$ cells take approximately 2 days on a Pentium® II 350 MHz processor. So, in order to decrease the turnaround time, we introduced two time steps

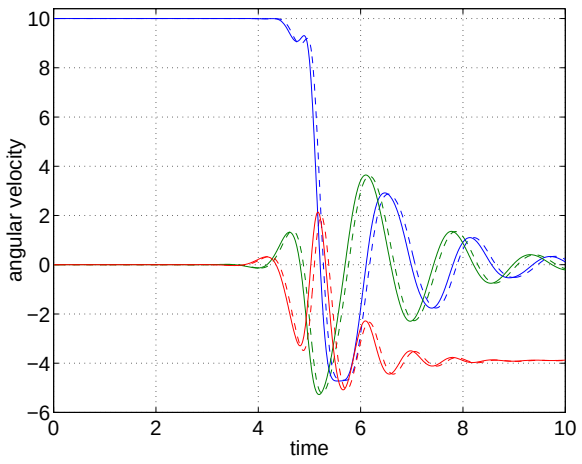

Figure 9: Same as Figure 7. The dashed lines correspond to multi time stepping.

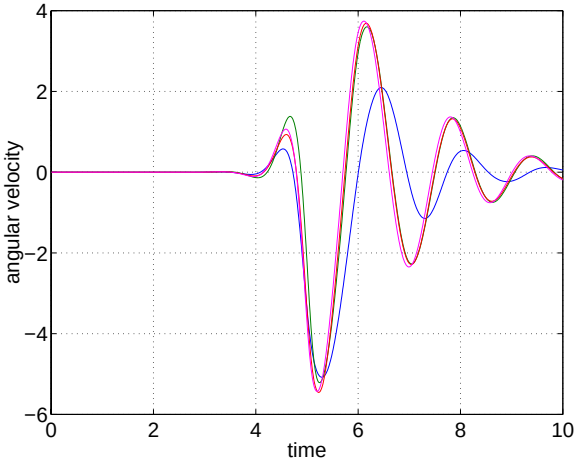

Figure 10: Angular velocity around the y-axis with time steps 2×10^{-3} (blue), 1×10^{-3} (green), 0.5×10^{-3} (red) and 0.25×10^{-3} (purple).

— one for the liquid model and a smaller one for the solid body model [9]. With multi time stepping [10], where the CFL-number in the liquid model is kept in the order 0.1 (which means that the time step in the liquid model is roughly a factor of 100 larger than

the time step in the solid body model), the same simulation as before can be performed overnight. In Figure 9 the consequences of multi time stepping on the results are shown, from which we conclude that multi time stepping has negligible effect on the accuracy. Therefore, the results of the following simulations have been produced using multi time stepping.

To check the effect of the time step we performed multiple simulations with different time steps. In Figure 10 the results of three simulations with time steps 2×10^{-3}, 1×10^{-3}, 0.5×10^{-3} and 0.25×10^{-3} are shown (note that these time steps refer to the liquid model; a time step 100 times smaller is used in the solid body model). For presentational reasons only the angular velocity around the y-axis is plotted.

To demonstrate the effect of the mass ratio we performed a simulation where the mass of the solid body was changed to $m_s = 48$. In this case the liquid mass corresponds to 50% of the total mass. The results are shown in Figure 11 and Figure 12. Note that, because

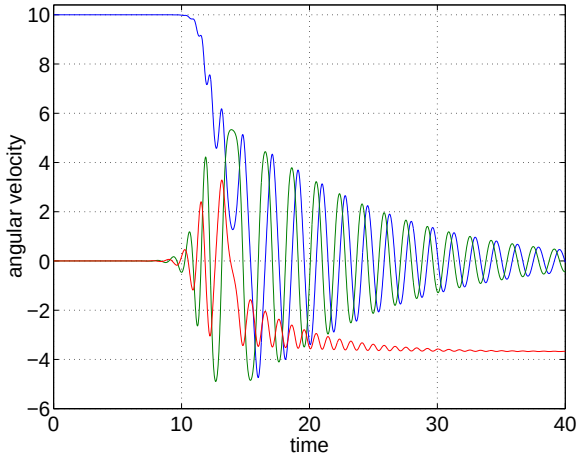

Figure 11: Same as Figure 7, but now with a liquid mass of 50%.

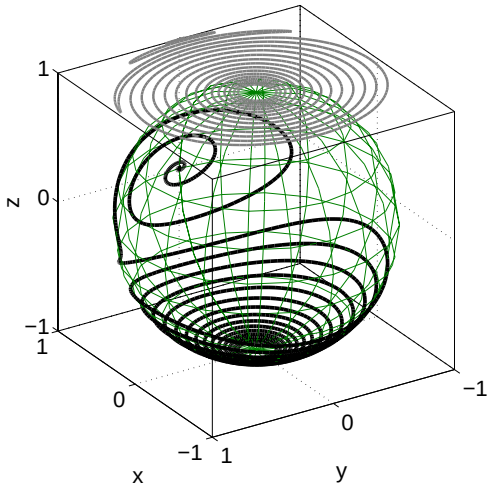

Figure 12: Same as Figure 8, but now with a liquid mass of 50%.

of the change in m_s, also the moment of inertia tensor of the solid body has changed, resulting in a (slightly) different final rotation rate, which should now be equal to 3.68. In our results the rotation rate around the z-axis tends to 3.67 (a difference of 0.3%). We observe that the time scale in the two simulations has changed a lot: in the case of a liquid mass ratio of 98% the change of rotation axis takes place in about 6 seconds, while this takes about 30 seconds in the case of a liquid mass ratio of 50%. Obviously, the effect of damping by the liquid has less effect if the liquid mass ratio decreases.

As a final example, we performed a simulation in which half of the container (again the rectangular tank of $6 \times 4 \times 2$) is filled with liquid. Initially, a block of fluid with dimensions $3 \times 4 \times 2$ is placed in the center of the tank. The density and the tank mass

are set to unity again, such that in this case $m_l/m = 96\%$. As before, initially, the system rotates around the (unstable) x-axis. The evolution of the angular velocities around the three principal axes is shown in Figure 13. Clearly, the behaviour of the coupled system

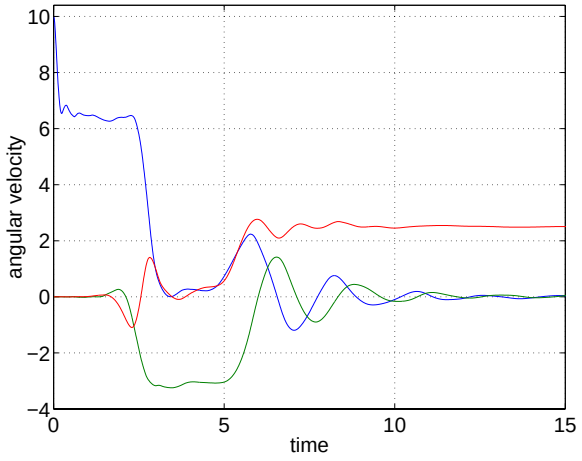

Figure 13: Same as Figure 7, but now the tank is partially filled with liquid.

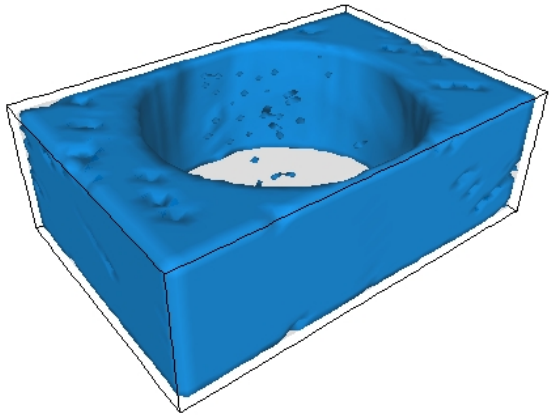

Figure 14: Snapshot (after 15 seconds) of the flat spin simulation where half of the tank is filled with liquid.

is very different from the previous simulations where the tank was completely filled with liquid. Although slightly more difficult (because of the free surface), also in this case, the final rotation rate around the z-axis can be computed. The simulation predicts a value of 2.51 which differs 0.4% from the theoretical value of 2.52. In Figure 14 a snapshot (after 15 seconds) of this simulation is shown. After 15 seconds the system is mainly rotating around the z-axis (the short axis), which explains the cylindrical shape (due to centrifugal forces) of the free surface.

We remark that the results show that our method is numerically stable, despite a very high liquid mass ratio of 50% or even close to 100%.

5 CONCLUDING REMARKS

In this paper we discussed a method for simulating the dynamics of coupled liquid-solid systems. The method consists of two parts: a model for the liquid dynamics and a model for the motion of the solid body. In the former, the solid-body motion appears as a force and torque in the Navier-Stokes equations, while in the latter the force and torque on the solid body that is induced by the sloshing liquid is embedded. A straightforward discretization of the equations for the solid body motion would result in a possibly unstable coupling, which has been illustrated with a simple mass-spring model. After rewriting the

equations, the resulting discretization proved to be stable for arbitrary liquid/solid mass ratios. Even if the mass of the solid body is negligible compared to the liquid mass, our method remains stable.

Since the time step is mainly limited by the solid body motion we incorporated a multi time stepping scheme in our method. This reduces the number of time steps in which the Navier-Stokes equations are solved and thus is extremely beneficiary for the turnaround time. Within the multi time stepping scheme we varried the size of the time step for convergence analysis. Also the effect of the liquid/solid mass ratio has been studied.

At present almost no validation material is available for the type of problems that we studied in this paper, whereas understanding the behavior of coupled liquid/solid sytems in micro-gravity conditions is very important: every satellite containing fuel is such a system. The experiment satellite SloshSat (see Figure 15) is such a satellite, which is scheduled for launch in 2001. It is designed to investigate liquid dynamics under micro-

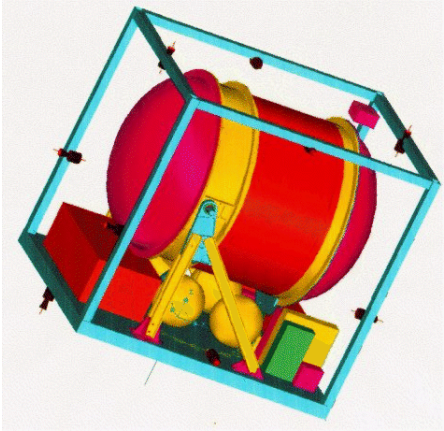

Figure 15: Mock-up of SloshSat.

gravity conditions and the interaction between the liquid motion and the motion of the solid body. SloshSat is a small free-flying satellite of which the Dutch National Aerospace Laboratory NLR is the main contracter. The experiment tank of SloshSat is a cylindrical container with hemispherical ends, having a volume of nearly 87 litres. The tank will be filled with approximately 33 litres of water representing a liquid mass that will be about 37% of the total mass. Currently, our method is capable of simulating the complete experiment scenario of SloshSat. With a successful flight of SloshSat we will therefore obtain valuable validation material for our method.

ACKNOWLEDGEMENT

J.G. wishes to acknowledge financial support from the Netherlands Organization for Scientific Research (NWO-SRON).

REFERENCES

[1] G. Fekken, A.E.P. Veldman and B. Buchner, *Simulation of green-water loading using the Navier-Stokes equations*, In: Proceedings 7th International Conference on Numerical Ship Hydrodynamics, Nantes, 19-22 July 1999, pp. 6.3-1–6.3-12 (1999).

[2] G. Yang, D.M. Causon and D.M. Ingram, "Cartesian cut-cell method for axisymmetric separating body flows", *AIAA J.*, **37(8)**, pp. 905–911 (1999).

[3] C.W. Hirt and B.D. Nichols, "Volume of Fluid (VOF) method for the dynamics of free boundaries", *J. Comput. Phys.*, **39**, pp. 201–225 (1981).

[4] M. Rudman, "Volume-tracking methods for interfacial flow calculations", *Int. J. Numer. Methods Fluids*, **24**, pp. 671–691 (1997).

[5] M.E.S. Vogels, *A numerical method for the simulation of liquid-solid body dynamics*, In: Proceedings 12th IMACS Congress, Paris, 18-22 July 1988 (R. Vichnevetsky, P. Borne and J. Vignes eds.), **2**, pp. 611–618, (1988). Also Report MP 87030 U, NLR, Amsterdam (1987).

[6] J. Gerrits, G.E. Loots, G. Fekken and A.E.P. Veldman, *Liquid sloshing on earth and in space*, In: Moving Boundaries V (B. Sarler, C.A. Brebbia and H. Power eds.), WIT Press, Southampton pp. 111–120 (1999).

[7] J.P.B. Vreeburg, *Free motion of an unsupported tank that is partially filled with liquid*, In: Microgravity Fluid Dynamics (H.J. Rath ed.), Springer, pp. 519–528 (1992).

[8] A.E.P. Veldman, "New quasi-simultaneous method to calculate interacting boundary layers", *AIAA J.*, **19**, pp. 79–85 (1981).

[9] K.C. Park and C.A. Felippa, *Partitioned analysis of coupled systems*, In: Computational methods for transient analysis (T. Belytschko and T.J.R. Hughes eds.), Elsevier Scientific Publishing Co., pp. 157–219 (1983).

[10] N.M. Maurits, H. van der Ven and A.E.P. Veldman, "Explicit multi-time stepping methods for convection-dominated flow problems", *Comput. Methods Appl. Mech. Engrg.*, **157**, pp. 133–150 (1998).